

## **Inductive Crosstalk Study of Embedded Current Sensor for SiC Die Current Measurement**

Meinert, Janus Dybdahl; Jorgensen, Asger Bjorn; Munk-Nielsen, Stig; Beczkowski, Szymon Michal; Andersen, Michael A.E.

*Published in:*

IEEE Journal of Emerging and Selected Topics in Power Electronics

*DOI (link to publication from Publisher):*

[10.1109/JESTPE.2024.3426610](https://doi.org/10.1109/JESTPE.2024.3426610)

*Publication date:*

2024

*Document Version*

Accepted author manuscript, peer reviewed version

[Link to publication from Aalborg University](#)

*Citation for published version (APA):*

Meinert, J. D., Jorgensen, A. B., Munk-Nielsen, S., Beczkowski, S. M., & Andersen, M. A. E. (2024). Inductive Crosstalk Study of Embedded Current Sensor for SiC Die Current Measurement. *IEEE Journal of Emerging and Selected Topics in Power Electronics*, 12(6), 5523-5533. <https://doi.org/10.1109/JESTPE.2024.3426610>

### **General rights**

Copyright and moral rights for the publications made accessible in the public portal are retained by the authors and/or other copyright owners and it is a condition of accessing publications that users recognise and abide by the legal requirements associated with these rights.






- Users may download and print one copy of any publication from the public portal for the purpose of private study or research.
- You may not further distribute the material or use it for any profit-making activity or commercial gain
- You may freely distribute the URL identifying the publication in the public portal -

### **Take down policy**

If you believe that this document breaches copyright please contact us at [vbn@aub.aau.dk](mailto:vbn@aub.aau.dk) providing details, and we will remove access to the work immediately and investigate your claim.



# Inductive Crosstalk Study of Embedded Current Sensor for SiC Die Current Measurement

Janus Dybdahl Meinert , Asger Bjørn Jørgensen , Stig Munk-Nielsen , Szymon Michal Bęczkowski  and Michael A. E. Andersen 

**Abstract**—Measuring the individual die currents in a multichip power module can aid in layout optimization, die selection and testing of current balancing strategies during the design phase. Thus, a two-stage current sensor concept with an embedded current transformer has been proposed. However, the magnetic crosstalk between the sensors and the layout and how it impacts the current sharing measurements has not been investigated. The embedded current transformers are in close proximity to the copper traces in the layout yielding parasitic magnetic couplings between each transformer and these traces. During switching the parasitic magnetic couplings are triggered yielding an extra contribution to the die current measurements, which impacts the accuracy of the current sensors. Ansys Maxwell is used to determine the strength of the different parasitic magnetic couplings between the current transformers and the nearby copper traces in the layout and a return wire is introduced for each transformer to mitigate the induced crosstalk. The return wire mitigation strategy is demonstrated and for the most crosstalk prone current transformer, a reduction in induced crosstalk from 7.3 to 2.8 % of the switched die current is achieved.

**Index Terms**—Current sensor, Crosstalk, Ansys Maxwell, FEM

## I. INTRODUCTION

HIGH bandwidth non-invasive current sensing solutions have gained increasing attention with the adoption of wide bandgap (WBG) semiconductor devices in power electronic systems [2]–[5]. WBG devices such as silicon carbide (SiC) offer higher blocking voltage, faster switching speed and increased operating temperature compared to conventional silicon [6], [7]. The advantages of SiC are obtained through power modules, i.e. compact integrated packaging solutions of bare SiC dies with a focus on minimizing layout parasitics in both the commutation and gate loops [8]. However, the compact packaging, low parasitic designs and faster device switching transients limits the selection of suitable high bandwidth physically small current sensing solutions applicable for local current measurements inside the power modules [9]. In case a high current capability of the power module is required, multiple dies are put in parallel. This further constrains the choice of applicable current sensors as the ability to perform individual die current measurements becomes a necessary feature. But studying the current sharing between the parallel

dies in a multichip module is a necessity to ensure a stable design where layout asymmetries or die variance are prone to cause uneven die stress [10], [11]. In order to measure the individual die currents inside a multichip power module the following features are essential when choosing a current sensing solution:

- Noise immunity: Due to the compact packaging, a power module is a complex electromagnetic environment where a high noise immunity is required of the current sensor to avoid potential sensor crosstalk and measurement inaccuracies [5], [12].
- Low insertion impedance: To reduce the sensor's impact on the measured switching transients, the insertion impedance of the current sensor has to be as small as possible [13].
- Galvanic isolation: To enable safe current measurements of both low-side and non-ground referenced high-side dies, galvanic isolation is a necessary attribute.
- High bandwidth: For SiC devices, risetimes in the range of a few tens of ns is obtainable which forces the current sensor to have a strong resolution up to hundreds of MHz to accurately capture the switching transients [14], [15].

In the literature, different current sensing solutions have been proposed that fulfil some of the above mentioned criteria. Commercially available current shunts offer bandwidths up to 2 GHz and by using an optical isolated voltage probe the galvanic isolation issue of the shunt can be dealt with [16], [17]. However, their physical size make them impractical for measuring current sharing between parallel connected dies inside a power module. In [18] a surface mount coaxial shunt resistor is developed that achieves a bandwidth of 2.23 GHz and deals with the size issue of the commercial current shunts. Their design also reduces the insertion inductance to 0.12 nH from the 2.3 nH introduced by the conventional current shunt [19]. The drawback of any shunt type current measurement is its intrusiveness in the commutation loop [20], and if the intention is to measure individual die currents in a power module it is necessary to have individual measuring planes for each current shunt which increases design complexity making the current shunt unfeasible. The Pearson current monitor provides galvanic isolation and with its bandwidth of 200 MHz it can accurately capture switching transients with risetimes below 10 ns [15], [21]. However, for individual die current measurements it suffers from its physical size and potential saturation issue at high current amplitudes [2]. The Rogowski coil has been the primary current sensing choice for evaluating

Manuscript created November, 2023; This paper is an extension of work originally presented at PCIM 2023 [1]. This work is supported by the Code project which is funded by the Poul Due Jensen Grundfos Foundation.

J.D. Meinert, A.B. Jørgensen, S. Munk-Nielsen and S.M. Bęczkowski are with AAU Energy, Aalborg University, Aalborg, Denmark ({jdm,abj,smn,sbe}@energy.aau.dk.). M.A.E. Andersen is with DTU Electro, Technical University of Denmark, Lyngby, Denmark, maea@dtu.dk

current sharing between parallel connected dies [22], [23]. The Rogowski coil does not suffer from saturation, it has galvanic isolation and meets the requirements of being non-intrusive as its insertion inductance is in the pH range [24]. Additionally, it has a high noise immunity due to its inherent winding configuration with a return wire as part of the design [25]. The primary limitation of the Rogowski coil is its 30 MHz, which is not adequate when the risetime of the device current nears 35-58 ns [26]. The bandwidth limitation of the commercial Rogowski coil is dealt with in [27], [28] where different variants of a PCB Rogowski coil concept are designed with bandwidths reaching 110 MHz and 58 MHz, respectively. Both [27], [28] are assessing the noise immunity of their designs based on the orientation of an outside neighbouring current and the distance between this current and their coil. With the inclusion of a return wire as in a commercial Rogowski coil, measurement errors from 5.5 % to as low as 0.2 % are demonstrated.

Due to the mentioned shortcomings of the current shunt solutions, the Pearson current monitor and the commercial Rogowski coil in relation to measuring individual die currents, a two-stage current sensor concept combining an embedded current transformer with a Pearson current monitor has been proposed in [1]. As for the commercial Rogowski coil, the two-stage current sensor is non-invasive as it does not require alterations of the circuit layout since the current transformers are embedded around the dies. The current sensor facilitates measurements of die currents with risetimes below 35-58 ns due to the higher 200 MHz upper bandwidth limit provided by the Pearson current monitor compared to using the commercial Rogowski coil with an upper bandwidth limit of 30 MHz. However the accuracy of the proposed two-stage current sensor concept and the performed current sharing measurements in [1] are uncertain as the noise immunity of the embedded current transformers has not yet been studied. In this paper the electromagnetic crosstalk between the two-stage current sensor's embedded current transformer and its surroundings will be investigated and how the crosstalk affects the accuracy of the current sensor will be assessed. In Section II, the working principle of the two-stage current sensor will be presented together with previous findings demonstrated in [1]. The size of the electromagnetic crosstalk for each embedded current transformer will be investigated in Section III at various voltage and current levels using double pulse tests (DPT). In Section IV Ansys Maxwell will be used to model the parasitic magnetic couplings between the layout and the embedded transformers. A crosstalk mitigation strategy is presented in Section V and Section VI concludes the results.

## II. TWO-STAGE CURRENT SENSOR WITH EMBEDDED CURRENT TRANSFORMER

The two-stage current sensor concept is composed of a Pearson current monitor and a current transformer with a customizable silicon steel core. Figure 1(a) shows a sketch illustrating the working principle of the two-stage current sensor with an embedded current transformer. The core of the embedded current transformer is encircling the die which

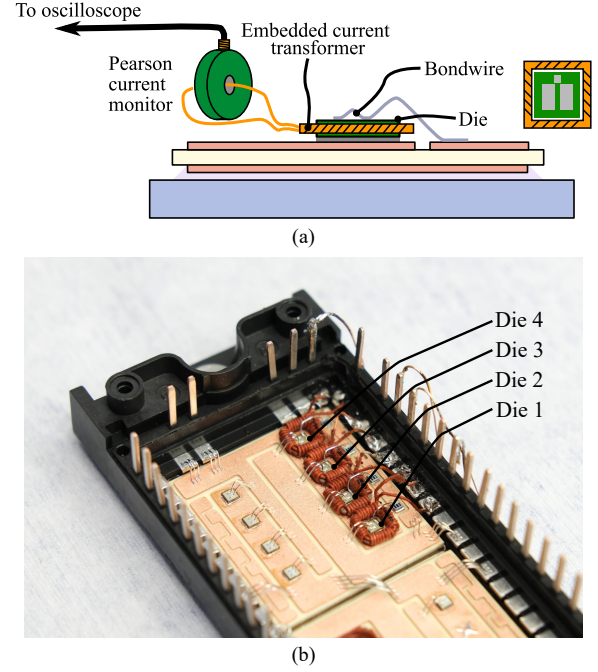


Fig. 1. (a) The concept of the two-stage current sensor [1]. (b) The designed power module for verifying the current sensor concept. The size of a current transformer is 6 mm x 6 mm x 1 mm.

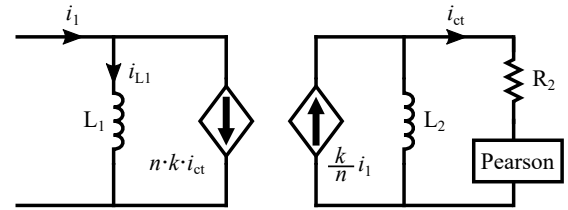


Fig. 2. The embedded current transformer is modelled using the current controlled current source equivalent transformer model [30, pp. 44–47]. The current  $i_1$  represents the drain current of the encircled die.

will behave as the primary winding of the transformer. The secondary winding of the transformer is shorted through a Pearson current monitor that is connected to an oscilloscope. During switching the generated magnetic field from the die current will be concentrated inside the transformer core and induce a current in the secondary winding of the current transformer. The current in the secondary winding is then read on the oscilloscope with the Pearson current monitor.

### A. Current Conversion Principle

For converting the transformer's secondary winding current ( $i_{ct}$ ) to the drain current of the die ( $i_1$ ), the following procedure is used. The droop effect and thus measurement error, which is caused by the transformer's leakage inductance, is taken into account by lifting the waveform, such that the current in the secondary winding is 0 A when the die is turned off [29]. The secondary winding current is next scaled using the gains presented in (1)–(2) which is derived from the current controlled current source equivalent transformer representation shown in Fig. 2 [30, pp. 44–47].

$$n = \sqrt{\frac{L_2}{L_1}} \quad k = \frac{M}{\sqrt{L_1 L_2}} \quad (1)$$

$$i_{ct} = \frac{sL_2 k}{(sL_2 + R_2)n} \cdot i_1 = \frac{k}{n} \cdot i_1 \quad \text{provided } sL_2 \gg R_2 \quad (2)$$

In the derivation it is assumed that the high frequency content of the switching current causes the impedance of the secondary side inductance to be much larger than the winding resistance during the switching transients. In addition it is assumed that  $i_{L1} \ll i_1$  such that  $nk i_{ct} \approx i_1$ .

From the analysis it is given that as long as the frequency content of the switching current satisfies the condition  $sL_2 \gg R_2$ , the induced current in the secondary winding will not be  $di/dt$  dependent but instead follow the die current.

### B. Demonstration of Two-stage Current Sensor

The two-stage current sensor concept is utilized to measure the current sharing in each of the four parallel dies in the power module seen in Fig. 1(b) during a DPT performed at 200 V and a total die current of 28.5 A. The switching waveforms are shown in Fig. 3 where a current sharing imbalance is seen between the four parallel dies prior to the turn-off and during the turn-on switching transients. The demonstrated imbalance during the turn-on switching transient is primarily due to the asymmetry of the layout that the dies are placed in. The dies are sharing the same gate driver but due to the asymmetry of the layout the size of the parasitic impedance in each specific die's gate driver loop is different. Especially the different common source inductances has an impact on the observed current sharing [10]. In addition, die variance might also have played a role as the dies were not binned prior to assembling the power module. However, other factors such as sensor variance and sensor crosstalk can have caused the current sharing between the dies to appear either more or less balanced than what is actually the case and thus influenced the acquired current sharing results. Potential sensor variance is dealt with by performing an impedance measurement of the current transformers from their secondary side prior to assembling the power module where the current transformers with the most resembling impedance curves are chosen. Regarding sensor crosstalk, the current transformers are in close proximity to parts of the layout (the drain and the source plane) which experience a high  $dv/dt$  and  $di/dt$  during the switching instances. In [1], the parasitic capacitive coupling between the drain plane and the secondary windings of the embedded current transformer has been studied and has not caused any measurement uncertainties within the investigated voltage levels.

In case a non negligible parasitic magnetic coupling is present between the layout and the embedded current transformers, the presented method in Section II-A for converting the measured secondary winding currents needs to be refined. The consequence of a parasitic magnetic coupling is an extra current contribution to the induced current in the secondary winding of a current transformer which is not considered in (2) when converting the measured secondary winding current of a current transformer to the actual die current. Depending on the strength of the parasitic magnetic coupling and the

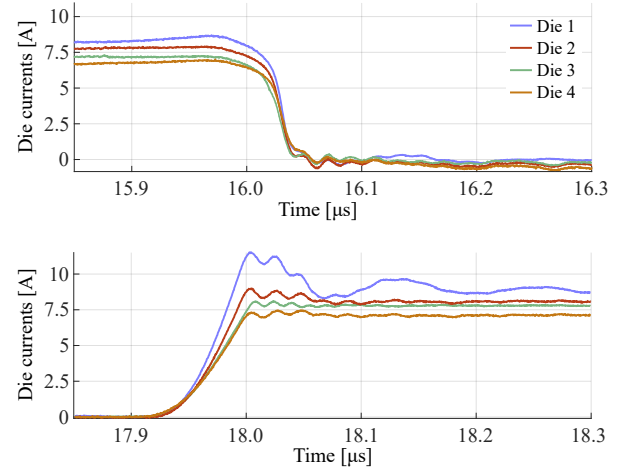


Fig. 3. The individual die current measurements from a DPT performed at an input DC voltage of 200 V and a total die current of 28.5 A.

alignment of its generated magnetic field, the induced noise current in the embedded current transformers can either be an added or subtracted contribution. With this contribution the current sharing can appear more or less balanced than what is actually the case. Whether any parasitic magnetic couplings between the embedded current transformers and the layout have deteriorated the sensors' accuracy and influenced the current sharing measurements shown in Fig. 3 has not yet been studied.

## III. INDUCTIVE CROSSTALK INVESTIGATION

The electromagnetic crosstalk between each current transformer and the layout will be investigated using a power module similar to the module presented in [1] and seen in Fig. 1(b).

### A. Experimental Setup

A 3D model of the module used for studying the electromagnetic crosstalk is seen in Fig. 4(a) and consists of a diode, four current transformers which are placed at the same positions as in the module used in [1] and a die with an externally connected gate driver circuit. Only one die is placed to isolate and analyze any crosstalk between the current transformers and the layout. A schematic of the setup is seen in Fig. 4(b) where the three current sensors under investigation are highlighted together with current sensor 3 that is used for measuring the die current.

The path of the die current is shown in Fig. 4(a) with the green line where it is via the drain plane going beneath current transformer 4. After which the current enters the source plane through die 3 and current transformer 3. In the source plane it borders one side of current transformer 2 and two sides of current transformer 1.

### B. Investigated Magnetic Couplings

The crosstalk is expected to be from couplings between both the source and drain planes to each sensor's transformer. How the common source plane is positioned around the

transformers can introduce parasitic magnetic couplings of different strength between the source plane and each current transformer. For the couplings between the drain plane and each transformer, the strength can be assumed identical as the four transformers are positioned nearly identical in relation to the drain plane in a four die design. With the experimental setup seen in Fig. 4(b) three different parasitic magnetic couplings are investigated. The first is the coupling between current transformer 1 and the source plane ( $\frac{n_{sct1}}{k_{sct1}}$ ), which describes the crosstalk induced in a current transformer when an adjacent current borders two sides of a current transformer. The second coupling is between the current transformer 2 and the source plane ( $\frac{n_{sct2}}{k_{sct2}}$ ), which describes the crosstalk induced in a current transformer when the transformer has one of its sides bordered by an adjacent current. The third coupling is between current transformer 4 and the drain plane ( $\frac{n_{dct4}}{k_{dct4}}$ ), which describes the crosstalk induced in a current transformer when a current goes beneath it.

The strength of the parasitic magnetic couplings are deter-

mined by comparing the die current measured with current sensor 3 to the measurements obtained from sensor 1, 2 and 4. The measured secondary winding current of current transformer 3 ( $i_{ct3}$ ) is scaled using the previously derived theory from [29], [30] with a coupling gain of  $\frac{n_3}{k_3} = 31.8$  which describes a transformer's magnetic coupling to its own die. For the measured secondary winding currents of current transformers 1, 2 and 4 ( $i_{ct1}$ ,  $i_{ct2}$ ,  $i_{ct4}$ ), the same theory is applied but the coupling gains are unknown. Instead the measurements will be scaled using the same gain as for current transformer 3 which yields the gains shown in (3)–(5).

$$i'_{ct1} = \frac{n_1}{k_1} \cdot i_{ct1} \quad i'_{ct2} = \frac{n_2}{k_2} \cdot i_{ct2} \quad (3)$$

$$i_3 = \frac{n_3}{k_3} \cdot i_{ct3} \quad i'_{ct4} = \frac{n_4}{k_4} \cdot i_{ct4} \quad (4)$$

$$\frac{n_1}{k_1} = \frac{n_2}{k_2} = \frac{n_3}{k_3} = \frac{n_4}{k_4} = 31.8 \quad (5)$$

By using these gains the impact of any crosstalk on a measured die current in a four die module is better visualized and by comparing switching current amplitudes, the actual coupling gains ( $\frac{n_{sct1}}{k_{sct1}}$ ,  $\frac{n_{sct2}}{k_{sct2}}$ ,  $\frac{n_{dct4}}{k_{dct4}}$ ) can be determined.

### C. Double Pulse Testing

The DPTs will be performed at 100 and 200 V and three different current levels 7.3, 10.7 and 14.1 A to ensure any observed crosstalk is entirely due to inductive couplings. The current transformers are glued to the drain plane and the tests are performed without the use of insulating gel. This enables the possibility to make minor adjustments to the current transformers at a later stage without changing their position or using another module. Leakage current test is performed in free air and showed safe operation up to 200 V.

The obtained results from the DPTs are seen in Figures 5 and 6. From Fig. 5 it is seen that when die 3 is turned on and off at both voltage inputs, a "switching transient" can also be observed in sensor 1, 2 and 4. This indicates that parasitic couplings are present between the layout and the embedded current transformers which are triggered during switching and inducing a crosstalk current into each transformers' secondary winding. The gradients of the die 3 current and the induced crosstalk current in sensor 1, 2 and 4 are aligned during both the turn-on and -off switching events. Thus it is evident that the induced die current in the secondary winding of a transformer and the induced crosstalk current will have the same positive direction and the crosstalk will be an added contribution to the measurements. In addition an "offset" is seen in the measured crosstalk current in sensor 1 and 2 prior to the turn-off and after the turn-on switching transients. The offsets are larger for sensor 1 than sensor 2 and thus seem to be dependent on the position of the embedded current transformers. These offsets due to crosstalk clarifies the observed spread between the measured die currents in Fig. 3 and has to be mitigated for future evaluation of current sharing between parallel dies.

A near voltage independence is observed when comparing the measured currents in all four sensors in Fig. 5 at the two input voltage levels. The rate of change in voltage is

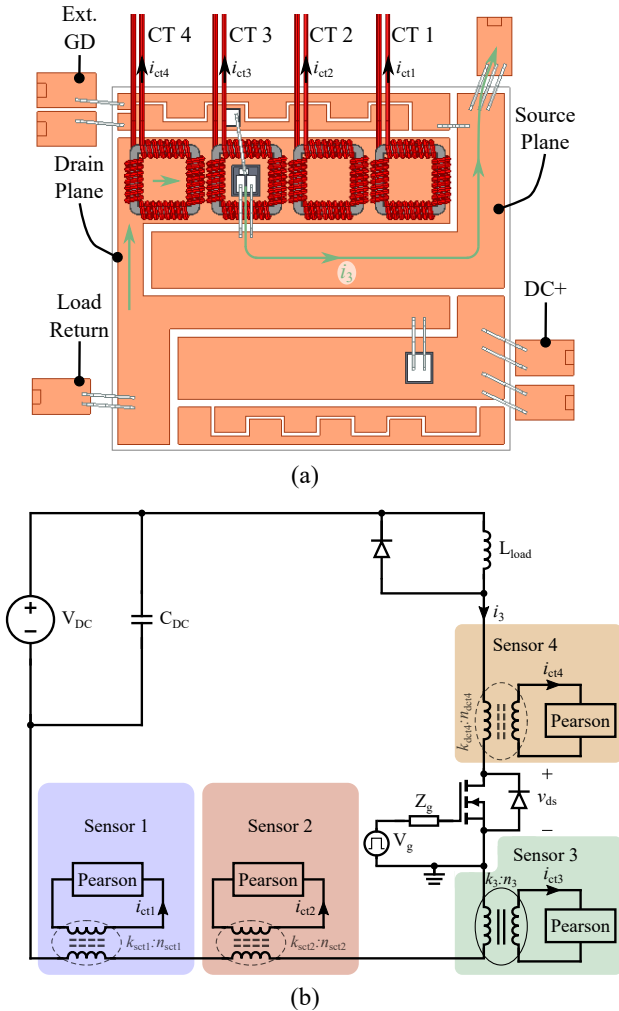


Fig. 4. (a) Top view of the 3D model of the power module used for determining the crosstalk between the layout and the embedded current transformers. The layout is identical to the module used in [1]. (b) Schematic of the experimental setup including the investigated parasitic magnetic couplings between the layout and current transformers 1, 2 and 4.

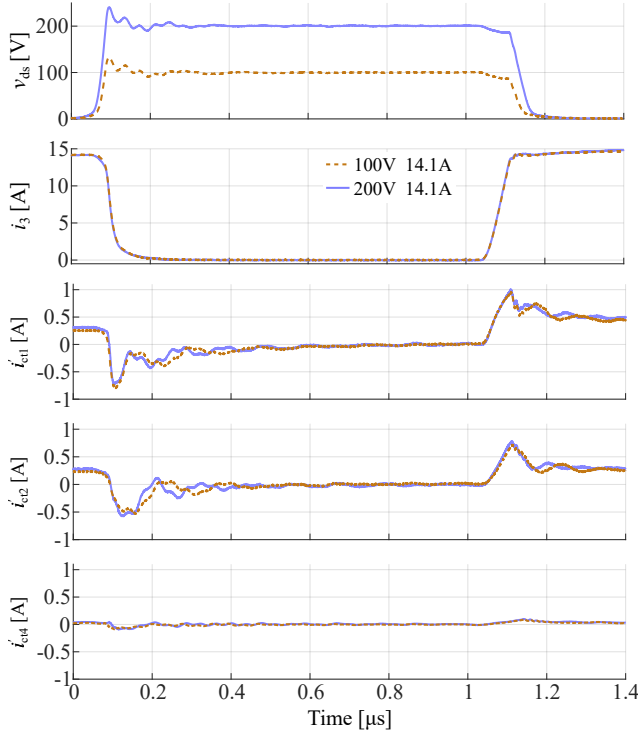


Fig. 5. Measured die current and crosstalk current seen by sensor 1, 2 and 4 at the DC input voltages of 100 and 200 V and a current level of 14.1 A.

approximately doubled when the input voltage is 200 V rather than 100 V, thus any current contribution to the total crosstalk caused by capacitive couplings should likewise be doubled. This implies that the observed crosstalk at the investigated input voltage levels is solely due to magnetic fields from the layout coupling to the three sensors.

An amplitude difference is observed between the measurements from sensor 1, 2 and 4 at any input voltage. This can be explained by two scenarios; either the coupling strengths between a respective current transformer and the layout are different or the coupling strengths are the same but the current triggering each coupling is different. As only one die is switched, the current in the circuit is known and it is the same current that goes beneath current transformer 4 and around current transformer 1 and 2, see Fig. 4(a). Thus, it can be concluded that the strength of each sensor's individual coupling to the layout is different and depends on the position of the respective sensor. The current path of the die current also dictates that the observed crosstalk current in sensor 1 and 2 is primarily due to parasitic magnetic couplings between their respective current transformer and the source plane of the layout as it is the part of the layout where the switched die current is nearest the two current transformers. The coupling between sensor 1 and the source plane is the strongest of the tested magnetic couplings whereas the one between the drain plane and transformer 4 is the weakest. The amplitude of the measured crosstalk of sensor 1 and 2 are approximately 12 and 9 times larger than the measured crosstalk of sensor 4 during the turn-on transient. Thus the couplings between the transformers and the source plane are dominant and the

TABLE I  
TURN-ON AMPLITUDES FROM FIG. 6 OF THE DIE CURRENT AND THE CROSSTALK CURRENT SEEN BY SENSOR 1 AND 2 AT AN INPUT DC VOLTAGE OF 200 V AND THREE DIFFERENT CURRENT LEVELS.

$i_3$	$\Delta i'_{ct1}$	$\Delta i'_{ct2}$	Induced crosstalk by die 3 current	
			$\left(\frac{\Delta i'_{ct1}}{i_3} \cdot 100\%\right)$	$\left(\frac{\Delta i'_{ct2}}{i_3} \cdot 100\%\right)$
7.3 A	0.55 A	0.41 A	7.5 %	5.6 %
10.7 A	0.80 A	0.60 A	7.5 %	5.6 %
14.1 A	1.03 A	0.77 A	7.3 %	5.5 %

TABLE II  
EXPERIMENTALLY DETERMINED GAINS FOR THE MAGNETIC COUPLINGS BETWEEN THE LAYOUT AND THE EMBEDDED CURRENT TRANSFORMERS.

Couplings between	Coupling gains (Experiment)
Dies and transformers	$\frac{k_1}{n_1} = \frac{k_2}{n_2} = \frac{k_3}{n_3} = \frac{k_4}{n_4} = 31.4e^{-3}$
Source plane and transformers	$\frac{k_{sct1}}{n_{sct1}} \approx 2.3e^{-3}$
	$\frac{k_{sct2}}{n_{sct2}} = \frac{k_{sct3}}{n_{sct3}} \approx 1.7e^{-3}$
Drain plane and transformers	$\frac{k_{dct2}}{n_{dct2}} = \frac{k_{dct3}}{n_{dct3}} = \frac{k_{dct4}}{n_{dct4}} \ll \frac{k_{sct1}}{n_{sct1}}$

dynamics introduced by the magnetic couplings between the drain plane and each transformer can in practice be neglected.

In Fig. 6 the measured currents in the die, sensor 1 and sensor 2 are shown at an input voltage of 200 V. The parasitic magnetic couplings between the source plane and the sensors 1 and 2 are analyzed at three different current levels and the read amplitudes during turn-on are shown in Table I. By comparing the crosstalk measurements in Fig. 6 and Table I of sensor 1 and 2 at the three different current levels a near linear trend is seen which reinforces the conclusion that the observed crosstalk is due to parasitic magnetic couplings between the source plane and the transformers. From the die current and the calculated relative difference between the crosstalk and the die current a set of magnetic gains  $\left(\frac{k}{n}\right)$  can be determined. The gains are shown in Table II and consist of the coupling factor and turns ratio describing the relation between the primary side and the secondary side current for each magnetic coupling.

The magnetic couplings of concern are; the intended couplings between each die and its respective current transformer, the unintended couplings between the source plane and a current transformer. The value for the magnetic gain describing the parasitic magnetic couplings between the drain plane and each current transformer are not included as the value is associated with some uncertainty due to the size of the measured sensor 4 crosstalk in Fig. 5. Additionally, the impact of the coupling between the drain plane and current transformer is negligible compared to the other couplings in the design. But for the couplings between the source plane and the current transformers, the size of the corresponding observed crosstalk in sensor 1 and sensor 2 is at a level where it cannot be ignored. In a four die design with similar layout if the crosstalk is not mitigated, its added contribution to each die current measurement will have an impact on any conclusions made in regards to the current sharing.

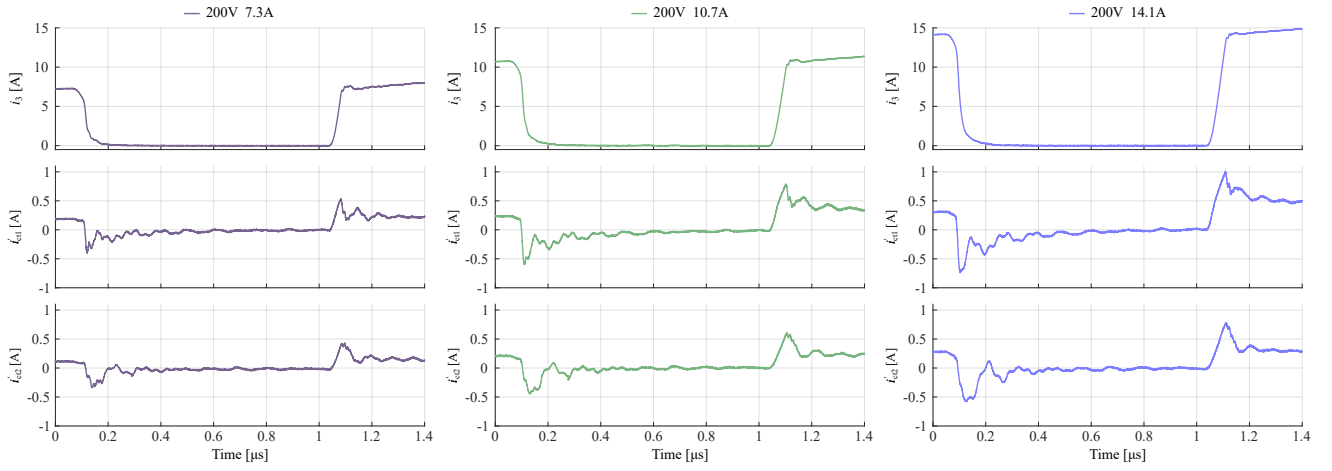


Fig. 6. Measured die current and crosstalk current seen by sensor 1 and 2 at an input DC voltage of 200 V and the current levels 7.3, 10.7 and 14.1 A.

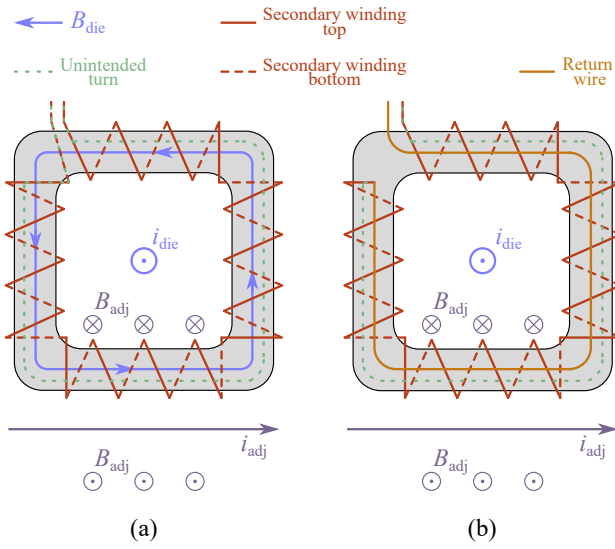


Fig. 7. Top view of sketched embedded current transformers where the die current and an adjacent current are shown including their respective magnetic fields. (a) Standard winding configuration. (b) Return wire winding configuration. [31]

In the following section Ansys Maxwell is used to study a 3D model of the power module to analyze how the source plane is coupling to the transformers and validate the strength of the observed parasitic magnetic.

#### IV. MODELLING OF PARASITIC MAGNETIC COUPLINGS

The strength of the observed parasitic magnetic couplings in the previous section was seen to depend on how big of a portion of a current transformers' sides is neighbouring the adjacent source plane current. The adjacent current behaves as the primary winding in the parasitic magnetic couplings and is linking to the unintended extra turn of the current transformer that comes as a consequence of wiring the cores.

In Fig. 7 the unintended turn is visualized by the dashed green line. The turn starts and ends at the wire ends of the actual secondary winding and is following the wiring direction of the secondary winding alongside the core's top surface. This extra turn does not link with the die current as it is in parallel to the magnetic field generated by the die current as seen in

Fig. 7(a). That is however not the case for the magnetic field from any adjacent current neighbouring the current transformer which will be perpendicular to the extra turn of the current transformer and will induce a crosstalk current in the current transformer.

In [27], [28] the same phenomenon is studied and a return wire is introduced to counteract the unintentionally created turn caused by winding the coil and thereby minimize the coupling to the neighbouring current.

In Fig. 7(b) the return wire strategy is shown for the embedded current transformers. The unintended turn is still present for the current transformer and is following the secondary winding wiring direction. But by returning the secondary wire in the opposite direction of the wiring direction, the effect the magnetic field from an adjacent current has on the unintended extra turn is nullified by the return wire. The ideal outcome of the return wire crosstalk mitigation strategy is zero crosstalk current from adjacent currents being induced in the secondary winding of the current transformer. This would lead to a secondary winding current of a current transformer to only consist of the contribution from the die current it is intended to measure and the expression in (2) being adequate for converting the secondary winding current of a current transformer to the actual die current.

By comparing Fig. 7(a) and (b), it is seen that both the unintended turn and the incorporated return wire are in parallel to the magnetic field from the die current encircled by the current transformer. Thus their influence on the current transformer's sensitivity in regards to measuring the actual die current encircled by the current transformer are negligible.

Lastly, as the core and the unintended turn are in parallel, the core will not impact the coupling between any adjacent current and the unintended turn. As a result, the adjacent current and unintended turn is solely linking through air which due to its non magnetic properties implies that the size of any induced crosstalk current is independent of the operating temperature.

#### A. Overview of Modelled Magnetic Couplings

The 3D model used for modelling the effect of this undesired turn and the parasitic magnetic couplings it causes is seen

Through an eddy current simulation in Ansys Maxwell the four coupling groups' contribution to the total induced secondary winding current of each transformer will be determined. The obtained coupling gains from the simulation depend on how the model is defined, thus this section presents a walk through of the model.

TABLE III

COMPARISON OF THE EXPERIMENTALLY DETERMINED AND SIMULATED GAINS FOR THE PARASITIC MAGNETIC COUPLINGS BETWEEN THE SOURCE PLANE AND THE EMBEDDED CURRENT TRANSFORMERS.

Coupling gains	Standard winding configuration (Experiment)	Full model standard winding configuration (FEM)	Crosstalk model standard winding configuration (FEM)	Crosstalk model return wire winding configuration (FEM)	Estimated crosstalk reduction (FEM)
$\frac{k_{sct1}}{n_{sct1}}$	$2.3e^{-3}$	-	$2.6e^{-3}$	$1.2e^{-3}$	54 %
$\frac{k_{sct2}}{n_{sct2}}, \frac{k_{sct3}}{n_{sct3}}$	$1.7e^{-3}$	$1.9e^{-3}$	$1.8e^{-3}$	$0.91e^{-3}$	49 %
$\frac{k_{sct1,i1}}{n_{sct1,i1}}$	-	$2.1e^{-3}$	$1.9e^{-3}$	$0.98e^{-3}$	48 %
$\frac{k_{sct2,i2}}{n_{sct2,i2}}, \frac{k_{sct3,i3}}{n_{sct3,i3}}, \frac{k_{sct4,i4}}{n_{sct4,i4}}$	-	-	$0.33e^{-3}$	$0.31e^{-3}$	6 %

1) *Defining the 3D model:* For each coupling the 3D model shown in Fig. 8 is cropped to include only the relevant current transformer, the part of the drain plane beneath it and the shaded area of the source plane corresponding to the coupling being investigated.

2) *The various current transformer 3D models:* Three models for the current transformer which include two different wiring designs will be studied. The three models are seen in Fig. 8(b) where (1) is the full transformer model with a standard winding configuration. Transformer model (2) also depicts a standard winding configuration. But it is distinguished by being designed to only model the crosstalk couplings by modelling the previously mentioned unintended turn that is created when wiring the core. Model (3) is also designed to only model the crosstalk couplings but a return wire is added as in a commercial Rogowski coil and the impact of this mitigation strategy on the measured crosstalk can be analysed.

3) *Choosing the solver frequency:* For the eddy current simulation an adaptive solver frequency or a frequency sweep have to be defined. As the current's distribution through the copper traces in the layout is frequency dependent, the distance between the primary winding in the source plane and the current transformer will likewise be it. This has the consequence that the strength of each coupling is frequency dependent. For the simulations in this paper the solver frequency is chosen by first investigating the coupling gains over a wide frequency range. Within the range a lower and upper boundary frequency is defined in which the chosen adaptive solver frequency has to lie. The aim is to know the strength of the couplings during the switching instants, thus the boundary frequencies are defined using the rise time of the measured crosstalk in Fig. 6 and (10) which describes the relation between risetime and bandwidth [14], [15].

$$f_{low} = \frac{0.35}{50 \text{ ns}} = 7 \text{ MHz} \quad f_{high} = 5 \cdot \frac{0.35}{50 \text{ ns}} = 35 \text{ MHz} \quad (10)$$

The investigated frequency range for two of the coupling gains is seen in Fig. 9 where the lower and upper frequency boundaries of 7 and 35 MHz are specified. It is seen that for both couplings that their gain is constant from above 70 kHz and thus also within the defined boundary region. As a result, the magnetic gains can be considered frequency independent during a switching transient which greatly simplifies the

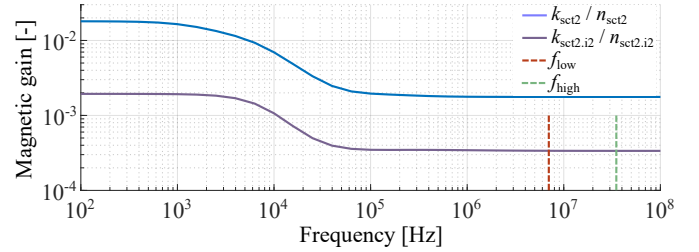


Fig. 9. FEM simulated coupling gains as a function of adaptive solver frequency. The gains are constant within the boundary defined by (10).

analysis and choice of solver frequency and thus 20 MHz is chosen.

4) *Simulation results:* In Table III the simulated coupling gains for the three different transformer models are shown and compared to the experimentally determined gains. First it is seen that the difference between using the full transformer model with standard winding configuration and the crosstalk model with standard winding configuration is between  $0.1e^{-3}$  and  $0.2e^{-3}$ . This is deemed to be insignificant when considering that the simulation results of the crosstalk model transformer representation are dependent on the position of single winding, the width of the winding and the height of the winding where all of these three parameters are estimates. Secondly a good agreement is seen between the experimental results and the simulated results of the standard winding configuration which implies that the unintended turn along the core is the root for the observed crosstalk. Comparing the crosstalk models with standard and return wire winding configurations it is seen that for three of the four set of couplings the inclusion of a return wire is a proper strategy for decreasing the coupling strength. It is only for the self-triggered couplings in the bottom row  $\left( \frac{k_{sct2,i2}}{n_{sct2,i2}}, \frac{k_{sct3,i3}}{n_{sct3,i3}}, \frac{k_{sct4,i4}}{n_{sct4,i4}} \right)$ , where the return wire does not add any noteworthy reduction. But the strength of these couplings is on a level where the crosstalk current they introduce is negligible.

## V. CROSSTALK MITIGATION STRATEGY

In the previous section the root cause of the crosstalk was demonstrated and the crosstalk mitigation strategy of using a return wire was tested in Maxwell where a reduction of 49 to 54 % was shown. In this section the mitigation strategy will be implemented and tested and the measurements compared to the results obtained in Section III.

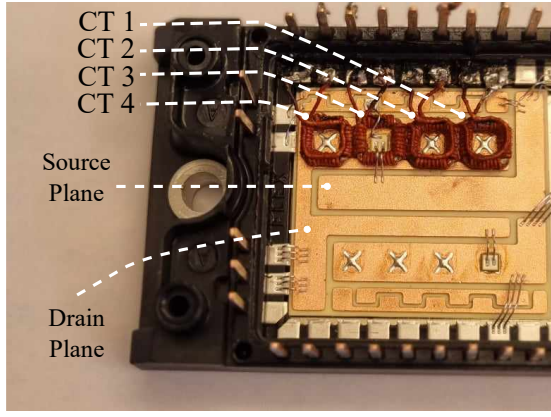


Fig. 10. The power module used for investigating the magnetic crosstalk between the layout and the current transformers. The current transformers 1, 2 and 4 have incorporated a return wire for mitigating the crosstalk.

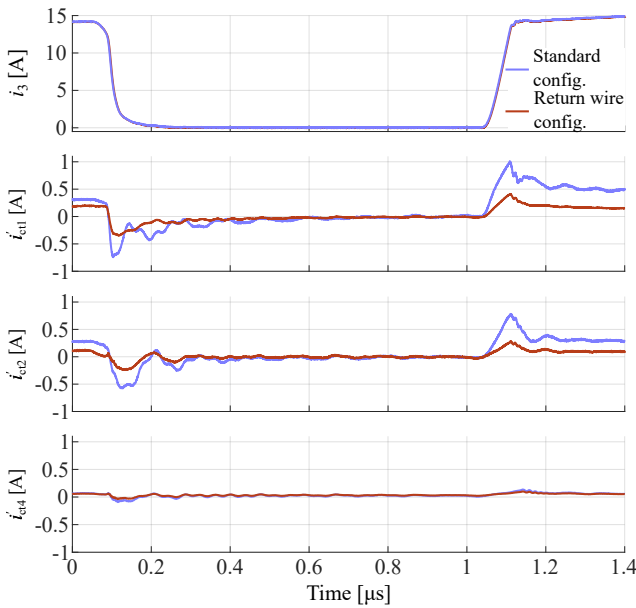


Fig. 11. Comparison of the standard and the return wire winding configurations in regards to the crosstalk current seen by sensor 1, 2 and 4. The comparison is performed at 200 V and 14.1 A.

In Fig. 10 the power module is shown where the return wire strategy has been implemented for current transformers 1, 2 and 4. The power module is the same as was used in Section III except for the implemented return wire. Thus the module only contains one die which is encircled by current transformer 3. Any current measured with current transformer 1, 2 and 4 will thereby be an induced crosstalk current. The measured secondary winding current of the current transformers are scaled using (3)–(5).

The comparison between the standard winding configuration design and the return wire winding configuration design is shown in Fig. 11 where a reduction in the induced crosstalk in current transformer 1, 2 and 4 is seen during both the turn-on and -off switching events. The crosstalk seen by current transformer 4 is still on a negligible level which reconfirms that the parasitic magnetic couplings between the drain plane and the current transformers can be ignored.

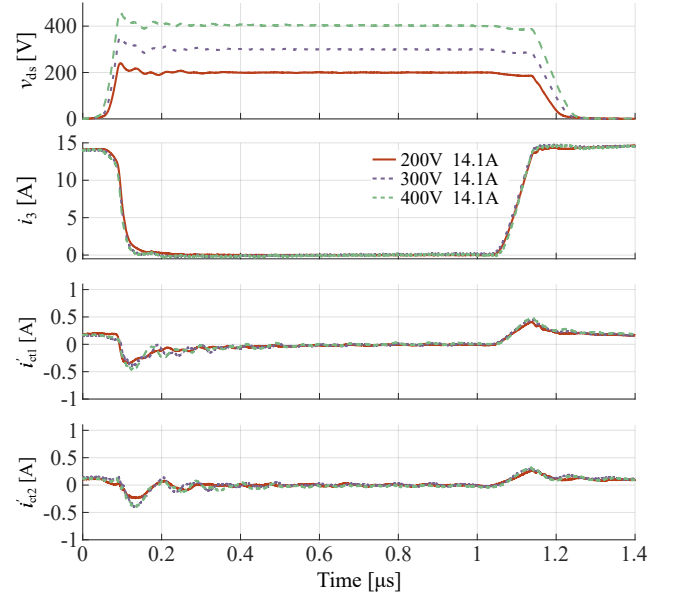


Fig. 12. Measured die current and crosstalk current seen by sensor 1 and 2 with the return wire winding configuration. The DC input voltages are 200, 300 and 400 V and the current level is 14.1 A.

In Fig. 12 the return wire winding configuration is tested at the input voltages 200, 300 and 400 V at a current level of 14.1 A. It is seen that the measured crosstalk current of current transformer 1 and 2 with the implementation of the return wire is still independent of the input voltage level.

A comparison of the turn-on amplitudes for the crosstalk current seen by current transformers 1 and 2 with and without the return wire at an input voltage of 200 V is shown in Table IV. The use of the return wire yields a relative change of the crosstalk by 62 and 64% between the two designs. This is a bigger improvement than what was estimated by the FEM simulations by 10 and 15 percentage points for the two types of couplings. With the use of the return wire the induced crosstalk by an adjacent current that adjoins two sides of a current transformer is lowered to 2.8%. For a current transformer which has one side neighbouring an adjacent current the induced crosstalk is reduced to 2.0%. These percentages are roughly the same potential measurement

TABLE IV  
TURN-ON CROSSTALK CURRENT AMPLITUDES FOR SENSOR 1 AND 2 FROM THE SENSOR DESIGN COMPARISON SHOWN IN FIG. 11.

	Standard winding configuration	Return wire winding configuration
$i_3$	14.1 A	14.1 A
$\Delta i'_{ct1}$	1.03 A	0.40 A
Induced sensor 1 crosstalk by die 3 current	7.3 %	2.8 %
Crosstalk reduction	62 %	
$i_3$	14.1 A	14.1 A
$\Delta i'_{ct2}$	0.77 A	0.28 A
Induced sensor 2 crosstalk by die 3 current	5.5 %	2.0 %
Crosstalk reduction	64 %	

errors that was presented by [27], [28] for their PCB Rogowski coils. Furthermore a measurement error of 2-2.8% due to a crosstalk contribution is acceptable as it is comparable to the measurement error of a commercial current probe e.g. the positional measurement accuracy of a commercial Rogowski coil [26].

## VI. CONCLUSION

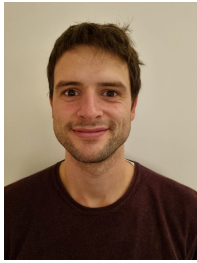
This paper investigates the crosstalk experienced by the embedded current transformers of four two-stage current sensors when they are used for measuring the die currents in a multichip power module. The crosstalk is studied through multiple double pulse tests, where a near linear trend is observed between the size of the induced crosstalk in the transformers and the amplitude of the switched die current, indicating parasitic magnetic couplings. It is identified using Ansys Maxwell that the parasitic magnetic couplings are between the transformers' unintended turn that is created when wiring their secondary winding and the neighboring sections of the source plane. A return wire is introduced as a solution to mitigate the crosstalk and depending on the position of the current transformers, reductions in the induced crosstalk from 7.3 to 2.8% and 5.5 to 2.0% of the switched die current are obtained. The current sensors' obtained measurement error between 2-2.8% due to crosstalk is within a typical probe measurement uncertainty.

## ACKNOWLEDGMENTS

This work was carried out under the CoDE project which is funded by the Poul Due Jensen Grundfos Foundation.

## REFERENCES

- [1] J. Meinert, S. Beczkowski, P. P. Kubulus, S. Munk-Nielsen, and A. B. Jorgensen, "Embedded current sensor for sic die current measurement," in *PCIM Europe 2023; International Exhibition and Conference for Power Electronics, Intelligent Motion, Renewable Energy and Energy Management*, 2023, pp. 1–8.
- [2] Z. Xin, H. Li, Q. Liu, and P. C. Loh, "A review of megahertz current sensors for megahertz power converters," *IEEE Transactions on Power Electronics*, vol. 37, no. 6, pp. 6720–6738, 2022.
- [3] Y. Shi, Z. Xin, P. C. Loh, and F. Blaabjerg, "A review of traditional helical to recent miniaturized printed circuit board rogowski coils for power-electronic applications," *IEEE Transactions on Power Electronics*, vol. 35, no. 11, pp. 12 207–12 222, 2020.
- [4] L. Shillaber, L. Ran, Y. Shen, and T. Long, "Gigahertz current measurement for wide band-gap devices," in *2020 IEEE Energy Conversion Congress and Exposition (ECCE)*, 2020, pp. 2357–2363.
- [5] A. Parsa Sirat and B. Parkhideh, "Current sensor integration issues with wide-bandgap power converters," *Sensors*, vol. 23, no. 14, 2023. [Online]. Available: <https://www.mdpi.com/1424-8220/23/14/6481>
- [6] B. Baliga, "Power semiconductor device figure of merit for high-frequency applications," *IEEE Electron Device Letters*, vol. 10, no. 10, pp. 455–457, 1989.
- [7] J. Hudgins, G. Simin, E. Santi, and M. Khan, "An assessment of wide bandgap semiconductors for power devices," *IEEE Transactions on Power Electronics*, vol. 18, no. 3, pp. 907–914, 2003.
- [8] J. K. Jorgensen, D. N. Dalal, S. Beczkowski, S. Munk-Nielsen, and C. Uhrenfeldt, "Multi-chip medium voltage sic mosfet power module with focus on low parasitic capacitance," in *CIPS 2020; 11th International Conference on Integrated Power Electronics Systems*, 2020, pp. 1–6.
- [9] A. B. Jørgensen, S. Munk-Nielsen, and C. Uhrenfeldt, "Overview of digital design and finite-element analysis in modern power electronic packaging," *IEEE Transactions on Power Electronics*, vol. 35, no. 10, pp. 10 892–10 905, 2020.
- [10] H. Li, S. Munk-Nielsen, X. Wang, R. Maheshwari, S. Beczkowski, C. Uhrenfeldt, and W.-T. Franke, "Influences of device and circuit mismatches on paralleling silicon carbide mosfets," *IEEE Transactions on Power Electronics*, vol. 31, no. 1, pp. 621–634, 2016.
- [11] G. Wang, J. Mookken, J. Rice, and M. Schupbach, "Dynamic and static behavior of packaged silicon carbide mosfets in paralleled applications," in *2014 IEEE Applied Power Electronics Conference and Exposition - APEC 2014*, 2014, pp. 1478–1483.
- [12] X. Chen, W. Chen, Y. Ren, L. Qiao, and X. Yang, "An advanced design of power module with emi reduction method," in *2018 IEEE Energy Conversion Congress and Exposition (ECCE)*, 2018, pp. 4671–4674.
- [13] S. Sprunck, C. Lottis, F. Schnabel, and M. Jung, "Suitability of current sensors for the measurement of switching currents in power semiconductors," *IEEE Open Journal of Power Electronics*, vol. 2, pp. 570–581, 2021.
- [14] X. Du, L. Du, Y. Chen, Y. Wei, A. Stratta, and H. A. Mantooth, "A nonlinear-model-based high-bandwidth current sensor design for switching current measurement of wide bandgap devices," *Sensors*, vol. 23, no. 10, 2023.
- [15] Tektronix. ABCs of Probes [Online]., <https://www.tek.com/en/documents/whitepaper/abcs-probes-primer>.
- [16] Current Viewing Resistors, T&M Research, [Online], <https://www.tandmresearch.com/index.php?page=products>.
- [17] IsoVu Isolated Probes, Tektronix, [Online], <https://www.tek.com/en/products/oscilloscopes/oscilloscope-probes/isovu-isolated-probes>.
- [18] W. Zhang, Z. Zhang, F. Wang, E. V. Brush, and N. Forcier, "High-bandwidth low-inductance current shunt for wide-bandgap devices dynamic characterization," *IEEE Transactions on Power Electronics*, vol. 36, no. 4, pp. 4522–4531, 2021.
- [19] S. Sprunck, M. Muench, and P. Zacharias, "Transient current sensors for wide band gap semiconductor switching loss measurements," in *PCIM Europe 2019; International Exhibition and Conference for Power Electronics, Intelligent Motion, Renewable Energy and Energy Management*, 2019, pp. 1–8.
- [20] S. Moser, M. Incurvati, M. Schiestl, and R. Stärz, "Non-invasive wide-bandwidth current sensor for wide-bandgap devices," in *2023 25th European Conference on Power Electronics and Applications (EPE'23 ECCE Europe)*, 2023, pp. 1–7.
- [21] Pearson Current Monitor 2877, [Online], <https://tmetrix.com/product/pearson-electronics-model-2877-current-monitors/>.
- [22] C. Zhao, L. Wang, F. Zhang, and F. Yang, "A method to balance dynamic current of paralleled sic mosfets with kelvin connection based on response surface model and nonlinear optimization," *IEEE Transactions on Power Electronics*, vol. 36, no. 2, pp. 2068–2079, 2021.
- [23] Y. Ge, Z. Wang, Y. Yang, C. Qian, G. Xin, and X. Shi, "Layout-dominated dynamic current balancing analysis of multichip sic power modules based on coupled parasitic network model," *IEEE Transactions on Power Electronics*, vol. 38, no. 2, pp. 2240–2251, 2023.
- [24] What is a Rogowski Coil?, [Online], <https://www.pemuk.com/how-it-works.aspx>.
- [25] The Basics of Rogowski Coil Current Probe, [Online], [https://www.pmk.de/web/editor/files/The%20Basics%20of%20Rogowski%20Coil%20Current%20Probe\\_Iwatsu%20AppNote.pdf](https://www.pmk.de/web/editor/files/The%20Basics%20of%20Rogowski%20Coil%20Current%20Probe_Iwatsu%20AppNote.pdf).
- [26] CWT Ultra-mini Rogowski Coil, [Online], [https://www.pemuk.com/Userfiles/CWTum/CWTUM\\_DS\\_Feb\\_2020.pdf](https://www.pemuk.com/Userfiles/CWTum/CWTUM_DS_Feb_2020.pdf).
- [27] M. Koga, M. Tsukuda, K. Nakashima, and I. Omura, "Application-specific micro rogowski coil for power modules - design tool, novel coil pattern and demonstration," in *CIPS 2016; 9th International Conference on Integrated Power Electronics Systems*, 2016, pp. 1–5.
- [28] S. Fu, X. Li, Z. Lin, Z. Zhao, X. Cui, X. Tang, and J. Wan, "Current measurement method of multiple chips using rectangular pcb rogowski coils integrated in press pack igt device," *IEEE Transactions on Power Electronics*, vol. 38, no. 1, pp. 96–100, 2023.
- [29] Q. Wu, K. Lu, and H. Li, "Modeling and analysis of current transformer for fast switching power module current measurement," in *2016 IEEE 8th International Power Electronics and Motion Control Conference (IPEMC-ECCE Asia)*, 2016, pp. 1615–1622.
- [30] K. Schuylenbergh and R. Puers, *Inductive Powering - Basic Theory and Application to Biomedical Systems*, 1st ed., ser. Hardcover. Springer, 2009, ISBN: 978-90-481-2411-4.
- [31] L. Ming, Z. Xin, W. Liu, and P. C. Loh, "Structure and modelling of four-layer screen-returned pcb rogowski coil with very few turns for high-bandwidth sic current measurement," *IET Power Electronics*, 01 2020.



**Janus Dybdahl Meinert** received the B.Sc. and M.Sc. degree in Energy Engineering with specialization in Power Electronics from AAU Energy, Aalborg University, Denmark, in 2019 and 2021, respectively. He is currently pursuing the Ph.D. degree with the same department. His research interests include design and analysis of current sensing solutions for individual die current measurements in multichip power modules, finite element simulation of electromagnetic interference and wide bandgap semiconductors.



**Michael A. E. Andersen** received the Master and PhD degrees in Power Electronics from the Technical University of Denmark, in 1987 and 1990, respectively. He is currently a Professor in Power Electronics at the Technical University of Denmark, where he has been Deputy Head of Department of Electrical Engineering from 2009-2022. He is the author and coauthor of more than 300 publications. His research group is very innovative with 76 filed inventions and 9 startup companies. He has been thesis advisor for 47 PhD students and more than 200 MSc students. His research interests include switch-mode power supplies, power converters, power factor correction, switch-mode audio power amplifiers, and VHF power converters. He also acts as an expert for the European Research Council.



**Asger Bjørn Jørgensen** received the M.Sc. and Ph.D. degrees in energy engineering from Aalborg University, Denmark, in 2016 and 2019, respectively. He is currently an Assistant Professor at AAU Energy, Aalborg University, Denmark. In 2015 he was a post-graduate student at University of New South Wales (UNSW), Australia and in 2018 a visiting researcher at the FREEDM Systems Center at North Carolina State University, USA. In 2020 he received the European Power Electronics and Drives Association (EPE) Outstanding Young EPE Member Award. His research is focused on power module packaging, wide bandgap power semiconductors and digital design using multi-physics finite element simulation.



**Stig Munk-Nielsen** received the M.Sc. and Ph.D. degrees in electrical engineering from Aalborg University, Aalborg, Denmark, in 1991 and 1997, respectively. He is currently working as a Professor WSR at the Department of Energy Technology, Aalborg University. He has been involved or has managed 12 research projects, including both national and European Commission projects. His research interests include low and medium voltage converters, packaging of power electronic devices, wide bandgap semiconductors, electrical monitoring apparatus for devices, failure modes, and device test systems.



**Szymon Michał Bęczkowski** received the M.Sc. degree in electrical engineering from the Warsaw University of Technology, Warszawa, Poland, in 2007. In 2012, he received the Ph.D. degree from Aalborg University, Aalborg, Denmark. He is currently working as Associate Professor at the Department of Energy Technology, Aalborg University. His research interests include LED drivers, power electronic converters, power module packaging and SiC technology.